

Modeling and experimental study on walking human-structure interaction systems subjected to earthquake excitations



Haowen Yang^a, Bin Wu^{b,c,*}, Guoshan Xu^{d,**}

^a Department of Structural Engineering, Tongji University, Shanghai, China

^b School of Civil Engineering and Architecture, Wuhan University of Technology, Wuhan, China

^c Sanya Science and Education Innovation Park of Wuhan University of Technology, Sanya, China

^d School of Civil Engineering, Harbin Institute of Technology, Harbin, China

ARTICLE INFO

Keywords:

Human-structure interaction
Real-time hybrid testing
Bipedal spring-loaded inverted pendulum
Human walking
Earthquake

ABSTRACT

The adverse effects of crowd activity on the structural response observed in several accidents have raised our concern about the role of human-structure interaction (HSI) on the seismic response of structures with dense crowds. To this end, a series of experimental campaigns and numerical studies have been conducted to investigate this phenomenon. In shaking table tests, participants walked individually on either a stationary or longitudinally vibrating treadmill, and their responses were measured. In particular, to better represent the HSI, a shaking table real-time hybrid testing (RTHT) was proposed and applied to evaluate the seismic response of the HSI system. A bipedal spring-loaded inverted pendulum (BSLIP) is then applied to simulate human behaviors. The experimental results indicated that the HSI in the longitudinal direction can be interpreted as additional positive mass and positive damping to the structure. Moreover, the RTHT showed that the human step frequency underwent significant changes when subjected to ground vibration, and synchronization occurred when the human step frequency was close to the structural vibration frequency, leading to a notable impact on the structural response. The numerical results show BSLIP model can represent both non-synchronization and synchronization responses of the human body, as well as effectively capturing the coupling between the longitudinal and vertical directions. Finally, the comparison between simulation and RTHT further confirms that the proposed BSLIP model is reliable to evaluate the seismic response of the HSI system.

1. Introduction

Human activities not only cause serviceability problems of civil engineering structures in terms of disturbing vibration, but also may induce safety problems [1]. In the London Millennium Bridge event, crowd walking triggered a large lateral vibration of the bridge deck, and the result of accident investigation attributed it to negative damping effects caused by human-structure interaction (HSI) [2]. A well-known event involving security is that Broughton Suspension Bridge in England collapsed due to dynamic instability induced by marching troops [3]. During Wenchuan Earthquake at 2:28 PM on May 12, 2008, many school buildings were severely damaged or collapsed while classrooms were filled with students. This naturally raises concerns about the safety of structures occupied

* Corresponding author at: School of Civil Engineering and Architecture, Wuhan University of Technology, Wuhan, 430070, China.

** Corresponding author at: School of Civil Engineering, Harbin Institute of Technology, Harbin, 150090, China.

E-mail addresses: wub@whut.edu.cn (B. Wu), xuguoshan@hit.edu.cn (G. Xu).

by dense crowds and subjected to earthquake excitation [4].

Walking away from buildings is the main manner of evacuation when earthquake intensity is large or crowds are dense. The human body is a sophisticated nonlinear system and cannot be simply regarded as an inertia mass [5,6]. On one hand, human walking induces structural vibration and changes structural dynamic properties [7]. On the other hand, the structural vibration in turn affects the human gait and hence human-induced forces [8]. Modeling the human body as a robot model is a natural way. For simplicity, the bipedal spring-loaded inverted pendulum (BSLIP) model has been widely used as a fundamental model for multi-rigid body robots and is believed to be able to generate natural gaits [9]. It was found that the BSLIP can generate more consistent results with human walking [10] when the forward movement of the center of pressure (CoP) is incorporated during stance. Currently, the BSLIP has been successfully applied to analyze HSI issues [11]. However, the BSLIP model cannot walk steadily without control when ground disturbances are large or damping is incorporated [12]. The human body is a feedback control system, and it controls its state by adjusting the muscle output according to perceptions of its state and ground vibration. Thus, the balance control strategy profoundly affects human responses and hence inevitably affects structural responses. Particularly, the balance behavior causes negative damping to structure [13,14] and even may lead to the synchronization phenomenon in the lateral direction [15]. The HSI in the longitudinal direction lacks relevant researches, and existing experimental results on the longitudinal balance behavior indicated the lower extremity muscles can sufficiently reduce the balance threat of anterior and posterior disturbances while trunk muscle activity is not necessary [16]. Therefore, although the BSLIP does not have a trunk, it is appropriate to represent balance behaviors on the longitudinally vibrating structure. To maintain stability, controllers need to be set on lower extremities, so the problem of modeling human behaviors converts to the problem of determining control parameters. Eventually, based on the inverted pendulum model, the crowd-structure interaction can be modeled by introducing the social force model [17], and the effectiveness of this approach was demonstrated in [18].

To study the seismic response of the HSI system, the numerical model is an important tool to accurately represent human behaviors, meanwhile, the innovative testing techniques are also helpful to better reflect HSI under earthquake excitations. Among test techniques, the shaking table test provides an approach to represent realistic human responses when subjected to different ground vibrations. However, the conventional shaking table test loaded according to pre-specified ground motion can only obtain the effects of structural vibration on the human walking gait, but cannot reflect the other aspects of HSI, that is, human walking cannot influence structural responses. Therefore, this article proposed a novel shaking table real-time hybrid testing (RTHT) that aims to study the seismic response of the HSI system that can consider both aspects of HSI. The RTHT was first proposed by Nakashima et al. [19] and now has been extensively applied in structural engineering to evaluate structural seismic performance. Horiuchi et al. performed the RTHT using a shaking table [20], and this technique has been further applied in structural vibration control [21], soil-structure interaction [22,23], train-track-bridge interaction [24], etc. As mentioned above, the human body is a highly nonlinear system with complex behaviors and control mechanisms. In general, the structural behavior is viewed as simpler, since its linear elasticity, elastic-plastic, and even geometrically nonlinearity can be well simulated by finite element methods. Therefore, in our RTHT, the human is taken as an experimental subsystem loaded on the shaking table while the structure as a numerical subsystem simulated in the computer, and the overall responses of the HSI system is ultimately obtained. Additionally, the test results are also used for validating the aforementioned BSLIP model.

This paper introduces the BSLIP model first and applies the classic PD control strategy to maintain stable walking. Then, it describes the shaking table tests that participants walked on either a stationary or a longitudinal vibrating treadmill. Based on these tests, the mechanism of HSI is studied, and the performance of the BSLIP model is verified. Finally, the seismic response of the HSI system was simulated by the RTHT, and the HSI system response is further validated based on BSLIP.

2. Dynamic model of human walking

2.1. Bipedal spring-loaded inverted pendulum model

The BSLIP for human walking depicted in Fig. 1 consists of a lumped mass on the center of mass (CoM), two massless spring legs with roller feet, and damping and actuator mechanisms. The mass is denoted by m_h , and the rest length and stiffness of the legs are denoted by l_0 and k_{leg} , respectively. The radius of the roller feet is set as $r_0=0.3l_0$ according to [10]. To avoid nonzero contact force at

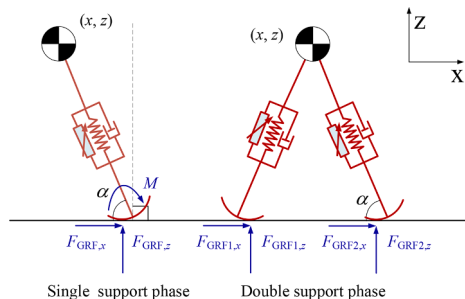


Fig. 1. SSP and DSP in the BSLIP model.

touchdown, the damping coefficients are assumed in proportion to deformation of legs. The model has two translational degrees of freedom (DoF), and the coordinate of the CoM is $[x \ z]^T$ in the global coordinate system. The position of the contact point between foot and ground $[x_{\text{foot}} \ 0]^T$ varies with rotation of the support leg. A human walking gait cycle contains a single support phase (SSP) and a double support phase (DSP), beginning with the touchdown of one foot and ending with the touchdown of another foot.

The control action is essential for stable walking. In the SSP, the force analysis for the support foot in Fig. 2 illustrates the ground reaction forces (GRFs) are composed of the distributed forces in the tangential and normal directions and can be idealized as a resultant force F and a moment M . Therefore, two virtual actuators are set, one is along the support leg to supply the axial control force, and the other is onto the support foot to generate the torque action. In contrast, human behaviors are more complex in the DSP than SSP. For simplicity, the torque action onto each foot is ignored and hence each leg contains only one actuator along the leg direction in the DSP.

In the DSP, the spring, damping, and control forces are all along the direction of the legs, as shown in Fig. 3. The spring forces are expressed as

$$f_{ds1} = k_{\text{leg}}(l_0 - l_1) \quad f_{ds2} = k_{\text{leg}}(l_0 - l_2) \quad (1)$$

where f_{ds} denotes the spring force in the DSP and the subscript '1' and '2' denote the trailing and leading leg, respectively;

$$l_1 = r_0 + \sqrt{(x - x_{\text{foot}1})^2 + (z - r_0)^2}, \quad l_2 = r_0 + \sqrt{(x - x_{\text{foot}2})^2 + (z - r_0)^2} \quad (2)$$

The damping coefficients are

$$c_{\text{leg}1} = 2m_h \sqrt{k_{\text{leg}}/m_h} \zeta(l_0 - l_1) / \Delta l_s, \quad c_{\text{leg}2} = 2m_h \sqrt{k_{\text{leg}}/m_h} \zeta(l_0 - l_2) / \Delta l_s \quad (3)$$

where ζ is the damping ratio and $\Delta l_s = m_h g / k_{\text{leg}}$ is the static displacement. Let

$$l_{s1} = \sqrt{(x - x_{\text{foot}1})^2 + (z - r_0)^2}, \quad l_{s2} = \sqrt{(x - x_{\text{foot}2})^2 + (z - r_0)^2} \quad (4)$$

The expression of \dot{l}_1 is

$$\dot{l}_1 = \frac{1}{l_{s1}} \left[(x - x_{\text{foot}1}) \left(-\frac{\partial x_{\text{foot}1}}{\partial x} \dot{x} - \frac{\partial x_{\text{foot}1}}{\partial z} \dot{z} + \dot{x} \right) + (z - r_0) \dot{z} \right] \quad (5)$$

where

$$\frac{\partial x_{\text{foot}1}}{\partial x} = \frac{(z - r_0)^2}{(z - r_0)^2 + l_{s1}^2 \sin \alpha / r_0}, \quad \frac{\partial x_{\text{foot}1}}{\partial z} = \frac{-(x - x_{\text{foot}1})(z - r_0)}{(z - r_0)^2 + l_{s1}^2 \sin \alpha / r_0} \quad (6)$$

The derivation of Eq. (6) is based on the following equations:

$$\begin{cases} (\alpha_1 - \alpha_{1,0})r_0 - (x_{\text{foot}1} - x_{\text{foot}1,0}) = 0 \\ \frac{(x_{\text{foot}1} - x)}{\sqrt{(x_{\text{foot}1} - x)^2 + (z - r_0)^2}} - \cos \alpha_1 = 0 \end{cases} \quad (7)$$

in which α denotes the inclination angle of legs, and the subscript '0' denotes the instant of touchdown. The expression of \dot{l}_2 is similar to that of \dot{l}_1 .

Because of roller feet, there are forces in the direction perpendicular to the legs. The corresponding perpendicular forces of spring and damping forces for the trailing and leading legs are

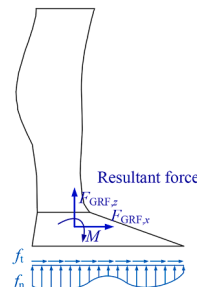


Fig. 2. GRFs on the support foot for SSP.

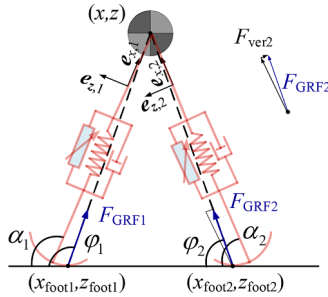


Fig. 3. Force analysis for the CoM.

$$f_{v,1} = -\tan(\varphi_1 - \alpha_1)(f_{ds,1} - c_{leg1}\dot{l}_1), f_{v,2} = -\tan(\varphi_2 - \alpha_2)(f_{ds,2} - c_{leg2}\dot{l}_2) \quad (8)$$

where φ_1 and φ_2 are the inclination angles between the connecting line of CoM and the contact point of the foot with the ground. The unit direction vectors of the trailing and leading legs are

$$\mathbf{e}_{x1} = [(x - x_{foot1}) \quad (z - r_0)]^T / l_{s1}, \quad \mathbf{e}_{x2} = [(x - x_{foot2}) \quad (z - r_0)]^T / l_{s2} \quad (9)$$

The unit direction vectors perpendicular to \mathbf{e}_{x1} and \mathbf{e}_{x2} are

$$\mathbf{e}_{z1} = [-\mathbf{e}_{x1}(2) \quad \mathbf{e}_{x1}(1)]^T, \quad \mathbf{e}_{z2} = [-\mathbf{e}_{x2}(2) \quad \mathbf{e}_{x2}(1)]^T \quad (10)$$

According to Newton's second law, the equations of motion of the CoM in the DSP are

$$\begin{bmatrix} m_h & 0 \\ 0 & m_h \end{bmatrix} \begin{bmatrix} \ddot{x} \\ \ddot{z} \end{bmatrix} = \begin{bmatrix} 0 \\ m_h g \end{bmatrix} + (f_{ds1} - c_{leg1}\dot{l}_1)\mathbf{B}_{h1} + (f_{ds2} - c_{leg2}\dot{l}_2)\mathbf{B}_{h2} + \mathbf{B}_h \mathbf{u} \quad (11)$$

where g is the gravitational acceleration; the control force $\mathbf{u} = [u_1 \ u_2]^T$, with u_1 and u_2 being the control forces of actuators; the configuration matrix \mathbf{B}_h is expressed as

$$\mathbf{B}_h = [\mathbf{B}_{h1} \quad \mathbf{B}_{h2}] = [\mathbf{e}_{x1} - \tan(\varphi_1 - \alpha_1)\mathbf{e}_{z1} \quad \mathbf{e}_{x2} - \tan(\varphi_2 - \alpha_2)\mathbf{e}_{z2}] \quad (12)$$

In the SSP, the control forces can also be transformed into the forces acting on the CoM by the configuration matrix \mathbf{B}_h [25]. With

$$\theta = \arctan[(x - x_{foot1})/z] = \arctan(\tilde{x}/z) \quad (13)$$

taking partial derivatives of θ with respect to its coordinates yields

$$\frac{\partial \theta}{\partial \tilde{x}} = \frac{z}{(x - x_{foot1})^2 + z^2}, \quad \frac{\partial \theta}{\partial z} = -\frac{(x - x_{foot1})}{(x - x_{foot1})^2 + z^2} \quad (14)$$

According to the principle of virtual work, the action of control moment can be transformed into two translational forces upon the mass, and correspondingly \mathbf{B}_{h2} in the SSP is given by

$$\mathbf{B}_{h2} = [\partial \theta / \partial \tilde{x} \quad \partial \theta / \partial z]^T \quad (15)$$

The expression of \mathbf{B}_{h1} is consistent to that in Eq. (12). Similarly, the equations of motion of the CoM in the SSP are expressed as

$$\begin{bmatrix} m_h & 0 \\ 0 & m_h \end{bmatrix} \begin{bmatrix} \ddot{x} \\ \ddot{z} \end{bmatrix} = \begin{bmatrix} 0 \\ m_h g \end{bmatrix} + (f_{ds1} - c_{leg1}\dot{l}_1)\mathbf{B}_{h1} + \mathbf{B}_h \mathbf{u} \quad (16)$$

In fact, Eqs. (11) and (16) can be written in a consistent form, and considering seismic input, they are in the form of state equation as

$$\dot{\mathbf{x}} = \begin{bmatrix} \dot{\mathbf{q}}_h \\ \mathbf{m}_h^{-1}(-\mathbf{f}_s - \mathbf{f}_d + \mathbf{f}_g) \end{bmatrix} + \begin{bmatrix} \mathbf{0} \\ \mathbf{m}_h^{-1}\mathbf{B}_h \end{bmatrix} \begin{bmatrix} u_1 \\ u_2 \end{bmatrix} + \begin{bmatrix} \mathbf{0} \\ -\mathbf{m}_h^{-1}\mathbf{u}a_g \end{bmatrix} \quad (17)$$

where $\mathbf{x} = [x \ z \ \dot{x} \ \dot{z}]^T$; $\dot{\mathbf{q}}_h = [\dot{x} \ \dot{z}]^T$; $\mathbf{f}_s, \mathbf{f}_d, \mathbf{f}_g$ are spring force, damping force and gravitational force, respectively; a_g is the horizontal ground acceleration.

The transition condition from the SSP to the DSP is that, during the fall of the CoM, it reaches a critical height

$$h_{TD} = (l_0 - r_0)\sin\alpha_{TD} + r_0 \quad (18)$$

with α_{TD} being the attack angle at touchdown, while the condition from the DSP to the SSP is that the trailing leg recovers to its rest

length.

2.2. Control strategy

The bipedal walking model has self-stabilization, but poor anti-disturbance ability [12,26]. When the damping is incorporated, the method of maintaining constant energy was used to achieve stable walking [11]. Visser et al. [26] proposed a variable leg stiffness control method to maintain a more stable walking of an undamped BSLIP, and so this study follows Visser's control method. First, let us define $\tilde{q}_1 = x - x_{\text{foot},v}$, where $x_{\text{foot},v}$ denotes the contact point position of the support foot in vertical leg orientation (VLO) during the SSP. The control error functions are $h_1(\tilde{q}_1) = z - z_d$ and $h_2(\tilde{q}_1) = v_x - v_{x,d}$, in which z_d and $v_{x,d}$ are desired height and velocity of the CoM, respectively. The desired gait is a function of the relative position \tilde{q}_1 because it is monotonically increasing in a gait cycle.

The generation of desired height and velocity curve needs to introduce the concept of the fixed point [25]. The model parameters are m_h , k_{leg} , l_0 , α_{TD} , and r_0 . Set $m_h=70$ kg, $l_0=0.95$ m, and $r_0=0.3l_0$ throughout the paper. The mass m_h and the length of legs l_0 are the average mass and 0.55 times [27] the average height of participants (detailed description in the subsequent test section), respectively. The state of VLO is chosen as the initial state with three independent variables: the height z_0 , the forward velocity v_0 , and the ratio of vertical and forward velocity δ_0 . For an undamped and uncontrolled BSLIP, beginning with the initial state, and going through a gait cycle, if the final state holds the following equations

$$\begin{bmatrix} z_1 \\ \delta_1 \end{bmatrix}^T = \begin{bmatrix} z_0 \\ \delta_0 \end{bmatrix}^T \quad (19)$$

the model can go back to the initial state owing to the conservation of energy. Correspondingly, the state can be defined as a fixed point. For the specified v_0 and δ_0 , it is seen from Eq. (20) that z_1 and δ_1 are the functions with respective to z_0 and α_{TD} , i.e.,

$$\begin{bmatrix} z_1(z_0, \alpha_{\text{TD}}) \\ \delta_1(z_0, \alpha_{\text{TD}}) \end{bmatrix}^T = \begin{bmatrix} z_0 \\ \delta_0 \end{bmatrix}^T \quad (20)$$

Newton's iteration method is usually applied to solve Eq. (19) and obtain z_0 and α_{TD} . And the analytical expressions of z_d and $v_{x,d}$ with respect to \tilde{q}_1 can be obtained by fitting the height and velocity responses corresponding to the fixed point [25].

Take the second and first time derivatives of error functions $h_1(x)$ and $h_2(x)$, respectively, and the derivations require Eq. (17) (refer to [25,26]); Then we can recast them in a compact form as

$$\dot{\mathbf{H}} = \mathbf{L} + \mathbf{A}\mathbf{u} \quad (21)$$

where $\mathbf{H} = [\dot{h}_1 \quad \dot{h}_2]^T$, the vector \mathbf{L} and matrix \mathbf{A} are determined by the expressions of the two derivatives [25]. Let $\mathbf{u}=\mathbf{A}^{-1}\mathbf{v}$, and the elements of \mathbf{v} are

$$v_1 = -k_{p1}h_1 - k_{d1}\dot{h}_1, \quad v_2 = -k_{p2}h_2 - k_{d2}\dot{h}_2 \quad (22)$$

where k_p and k_d are the control parameters.

2.3. Control effect

In this part, simulations of uncontrolled and controlled BSLIP models are conducted with model parameters of $k_{\text{leg}}=23$ kN/m, $\zeta=0.0$, $\alpha_{\text{TD}}=67.52^\circ$; initial states of $z_0=0.9279$ m, $v_0=0.995$ m/s, $\delta_0=0$; and the integration time interval of $\Delta t=0.0001$ s. Fig. 4(a) is

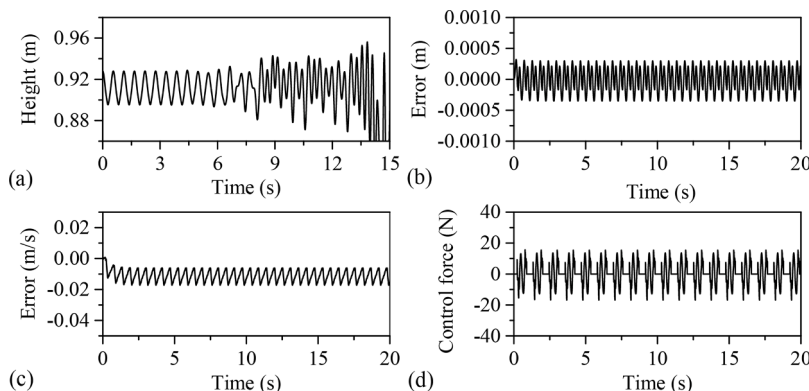


Fig. 4. Uncontrolled and controlled BSLIP model; (a) height of the CoM - uncontrolled, (b) height tracking error, (c) velocity tracking error, and (d) control force of the leg actuator.

the height time history of the CoM for the uncontrolled model. It can be observed that the uncontrolled model cannot walk steadily even without damping, and gradually lost its stability after 6 s. Fig. 4(b) and (c) are the tracking errors of height and velocity for the controlled model with model damping $\zeta=0.06$. The tracking errors are relatively small with constant range of variations. This indicates that the controlled model can walk steadily even accounting for damping and hence the control improves the stability effectively. The vertical control force of a leg acting on the CoM is small as expected owing to the low damping ratio as shown in Fig. 4(d). The control parameters adopted in the simulation are $k_{p1}=150$, $k_{d1}=30$, $k_{p2}=2.5$ and $k_{d2}=0.18$.

3. Shaking table tests

3.1. Experimental setup

In the conventional shaking table tests, participants individually walked on a treadmill that was fixed on a frame, the two together called a treadmill system, as shown in Fig. 5. The treadmill system was suspended from a base frame by four hinges and the base frame was anchored on the shaking table using high strength bolts. The vertical force of the frame system and participant was sustained by these hinges, while the longitudinal and lateral forces can be transmitted to four load cells. The longitudinal force and acceleration were measured by four load cells and an accelerometer, respectively. Therefore, the longitudinal walking force can be calculated by the following formula

$$F_{\text{longitudinal}} = \sum_{i=1}^4 F_{m,i} - m_{ts}a_{ts} \quad (23)$$

where $F_{m,i}$ denotes the measured force by the i th sensor; m_{ts} and a_{ts} denote the mass and acceleration of the treadmill system, respectively. Detailed descriptions of the measurement of walking force are seen in [25,27,28]. Before the tests, the load cells were verified by standard masses. The displacement and acceleration signals were collected by a linear variable differential transformer (LVDT) and a KD1300 accelerometer, respectively. The displacement, acceleration, and longitudinal forces were collected by a DH5922 with a sampling frequency of 1000 Hz. The vertical ground reaction force was collected by Novel loadsol® with a sampling frequency of 100 Hz. Actual measured belt speed demonstrated negligible variation caused by human walking, so the longitudinal force can be considered to be the same as the force that the participants walk on the ground.

3.2. Test procedures

The shaking table tests contained two steps as follows

- (1) Walking tests were conducted on the stationary treadmill to investigate the mechanical responses of human body and to obtain step frequencies at different speeds, as a foundation for the subsequent study.
- (2) Walking tests were conducted on the longitudinally vibrating treadmill and shaking table inputs were sinusoidal waves with the frequencies $f_b=1.6\text{-}2.0$ Hz around the human step frequencies and amplitudes of 10 mm, 15 mm, and 20 mm. These tests were used to obtain the human walking force responses and hence study balance mechanisms under disturbances.

All participants had a weight of 69.4 ± 11.1 kg and a height of 1.73 ± 0.03 m. The details are listed in Table 1. These tests were conducted in accordance with the Code of Ethics of the World Medical Association (Declaration of Helsinki) for experiments involving human participants.

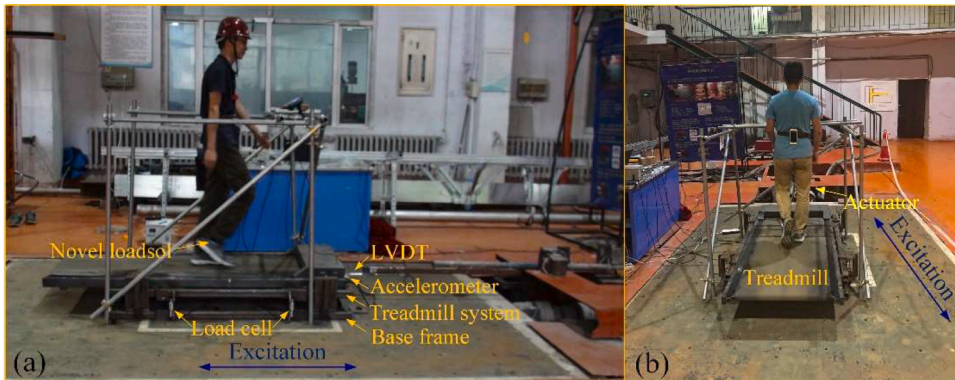


Fig. 5. Test scenarios, (a) lateral view and (b) back view.

Table 1
Participants' height and mass.

Participant	A	B	C	D	E	F	G
Height (m)	1.76	1.68	1.72	1.70	1.75	1.75	1.77
Mass (kg)	75.2	51.8	61.7	70.0	68.0	71.7	87.5

3.3. Test results and model verification

3.3.1. Walking on the stationary treadmill

The longitudinal force profile exerted on the ground in one single step can be divided into two parts: the force is forward and its reaction force represents braking force when the forefoot touched the ground; the force is backward and its reaction force represents propulsion force when the CoM crosses the CoP. All longitudinal force data were filtered by a Butterworth low-pass filter with a cut off frequency of 8 Hz. Fig. 6(a) displays a time history of nominal longitudinal force (normalized by the participant's weight) for the participant walking at the speed of 1.07 m/s. Its Fourier spectrum (Fig. 6(b)) had large components at the step frequency of 1.8 Hz and higher harmonics, and the first three order dynamic load factors (DLFs, which are defined as Fourier coefficients of harmonics [1]) decreased in turn. Fig. 6(c) and (d) are the simulated longitudinal force by the BSLIP model and its Fourier spectrum. The model parameters and control parameters follow those parameters used for the cases in Fig. 4, and the step frequency and speed are selected to be consistent with the test. It can be observed that the magnitude of the longitudinal force and the first three order DLFs agree with the test. Nevertheless, Fig. 6(c) illustrates that the magnitude of the longitudinal force is constant, so the simulation does not represent the intra-subject variability.

For all the first step shaking table tests, the longitudinal and vertical walking forces were measured at the speed of 0.78-1.94 m/s. Participants walked on their preferable step frequencies increased with walking speeds in the range of 1.6-2.4 Hz. The first two order DLFs in Fig. 7 demonstrate that the magnitude of longitudinal force increased nearly linear with velocity. The maximum longitudinal force magnitude reached 0.3 times the weight of participants. However, the magnitude no longer grew and even showed a decreasing trend when the walking speed exceeded 1.7 m/s. The test results are also consistent with those of Kumar et al [29]. Then simulations are performed with the leg stiffnesses of 20 kN/m and 23 kN/m, and the corresponding dimensionless leg stiffnesses ($k_{\text{leg}}/m_{\text{leg}}g/l_0$) are consistent with [30]. Fig. 7 also shows the step frequencies for different leg stiffnesses and speeds, and connects the DLFs for same leg stiffnesses and step frequencies with lines. The simulation results show that longitudinal forces and step frequencies are in

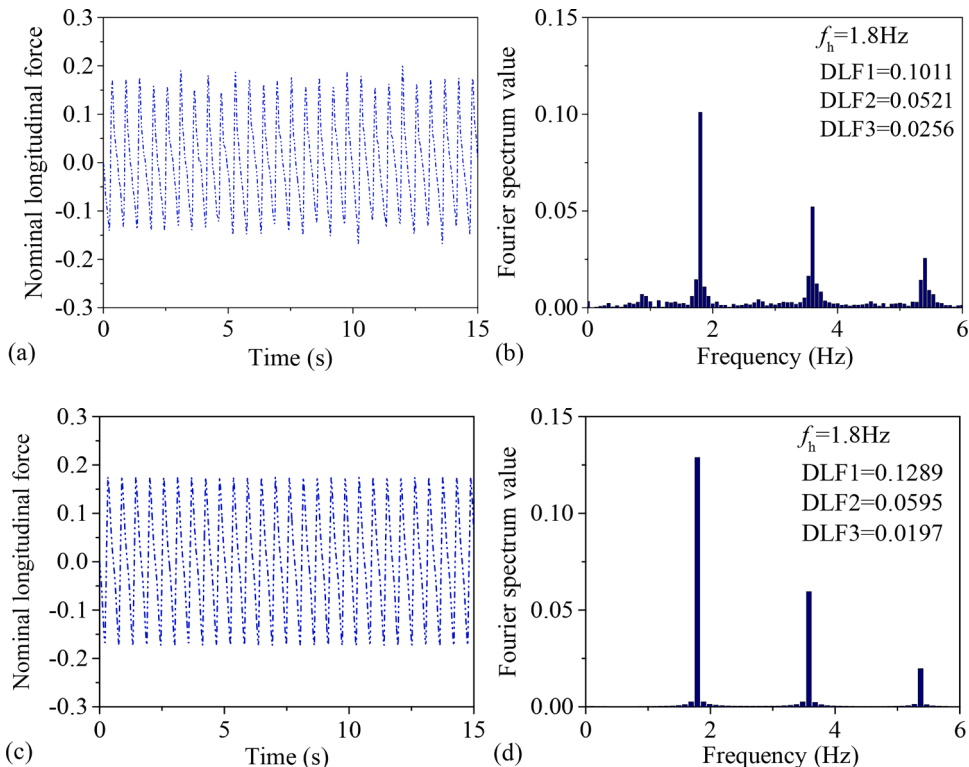


Fig. 6. Test and simulation results for walking on the stationary surface; (a) experimental time history of longitudinal force; (b) Fourier spectrum of experimental force data; (c) simulated time history of longitudinal force; (d) Fourier spectrum of simulated force data.

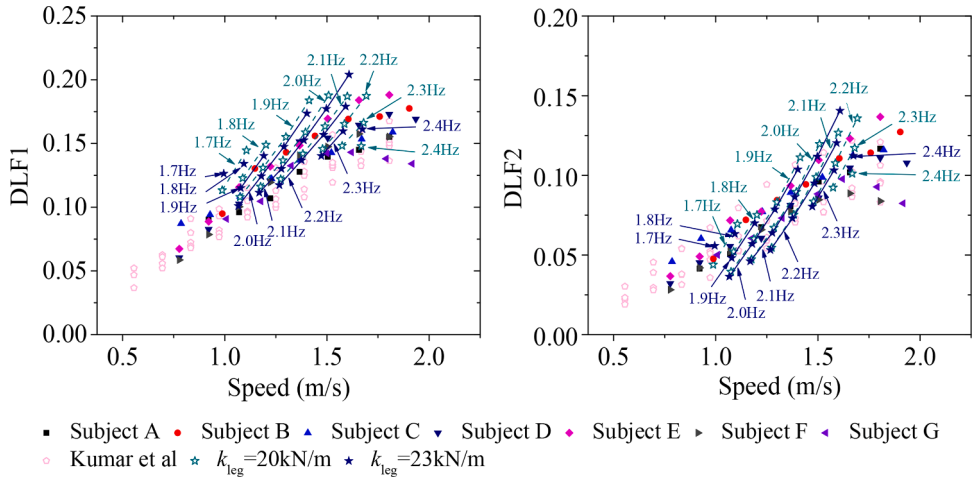


Fig. 7. Longitudinal DLFs at different speeds.

good agreement with those of the tests, indicating that the BSLIP model can represent the characteristics of longitudinal force well. It can be also seen that the first two order DLFs decrease with the increase of the step frequency at the same speed, while the first two order DLFs increase with increasing the leg stiffness at the same speed and step frequency.

Besides the step frequency and DLF, another important factor is the ratio of SSP and DSP. With the walking period t_1 and the duration from one foot touching the ground to this foot leaving the ground t_2 , define $\beta = t_1/t_2$ [12], knowing that $\beta=1$ denotes that only the SSP exists, as seen in the walking model with the rigid legs [13]. Each participant was tested at seven different speeds with the range of 0.92–1.92 m/s. The vertical force time history of 30 continuous gaits was recorded (15 for the left foot and 15 for the right foot), and hence a total of 1470 gaits were collected. Then t_1 and t_2 can be obtained and β can also be computed. In Fig. 8, each scatter point denotes an average value of β for the successive left and right foot steps, and each line denotes the average value of each participant. Fig. 8 shows that β slightly increased with the speed, which means that the DSP ratio decreased. β was in the range of 0.759–0.894 and its average value was at 0.788–0.876. For comparison, simulation results of β corresponding to the gaits in Fig. 7 are also depicted in Fig. 8 and marked with pentagrams. It is seen that simulated β values are basically consistent with experimental results.

3.3.2. Walking on the longitudinally vibrating treadmill

Under the excitation of sinusoidal waves, the longitudinal force showed significant change compared with that of walking on the stationary treadmill and had large differences to take a human as an inertia mass. Fig. 9(a) is a typical time history of the longitudinal force at the walking speed of 1.07 m/s and the step frequency f_h of 1.852 Hz, in which the excitation frequency f_b was 1.6 Hz with measured amplitudes of displacement and acceleration of 19 mm and 1.91 m/s², respectively. And the walking forces represented

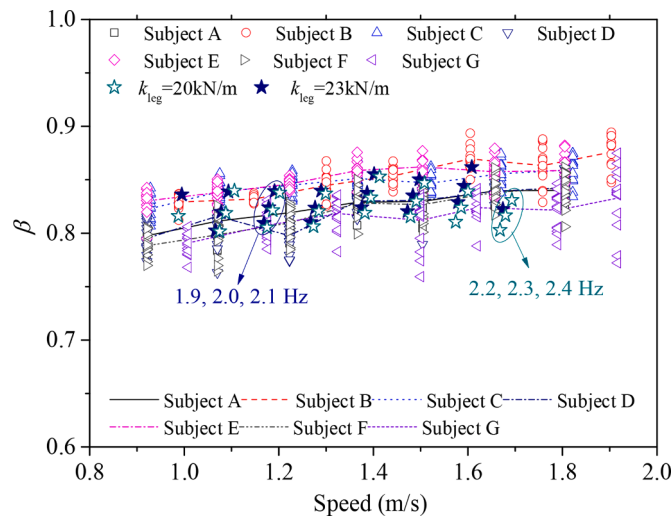


Fig. 8. β at different speeds

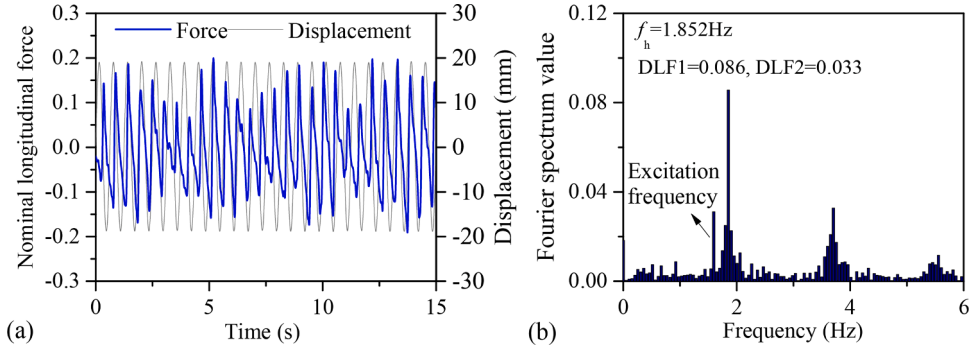


Fig. 9. Test results for walking on a vibrating surface; (a) longitudinal force and (b) Fourier spectrum.

periodic variations with the beating frequency being the absolute value of the difference between step frequency and excitation frequency, that is, $\delta_f = |f_h - f_b|$, as in Fig. 9(a). From Fig. 9(b), it can be observed that the harmonic components of the Fourier spectrum of the longitudinal force were lower than that of Fig. 6(b). Sideband force components appeared on both sides of the main harmonic, and the component at excitation frequency was larger than that at the other side. Around higher order harmonics, sidebands [31] were not obvious.

By analyzing the cases that participants did not synchronize with the excitations, the average value of the peak longitudinal force did not change, while the interaction force (reported in [25]) increased with the vibration velocity amplitude as shown in Fig. 10(a), and the linear fitted relationship is also depicted in Fig. 10(a). The phase angles that the human longitudinal force lags the shaking table displacement when the force reaches beating peak, as shown in Fig. 10(b), were mostly distributed between 0° – 90° , which means that the interaction force can be interpreted as positive mass and positive damping.

3.3.3. Model validation

3.3.3.1. Excitation frequency is lower than step frequency. The maximum longitudinal force appeared first in the positive direction when the excitation frequency was lower than the step frequency; while the maximum value appeared first in the negative direction when the excitation frequency was higher than the step frequency; this is due to the influences of the higher order DLFs. The longitudinal force of the test and its simulation counterpart under the excitation frequency of 1.6 Hz and amplitude of 19 mm are depicted in Fig. 11(a). It can be seen that the occurrence of the maximum longitudinal force intervals several gait cycles and the simulated longitudinal force coincides with the test in both magnitude and shape, demonstrating that the control mechanism is reasonable. Test results on the stationary treadmill can be used to calibrate the model parameters, while test results on the vibrating treadmill can be further used to calibrate the control parameters. The Fourier spectrum of the simulated longitudinal force in Fig. 11(b) shows that the first-order DLF is slightly larger than that of the test. Some other frequency components occur around the harmonics because the step frequency changed slightly when the model is subjected to ground vibration, and this attenuates the amplitude of the dominant frequency components. The sideband force component related to excitation appears at 1.6 Hz, consistent with the test in Fig. 11. The sidebands are not obvious around higher-order harmonics owing to the variation of the step frequency. The model parameters adopted in the simulation: $k_{\text{leg}}=23 \text{ kN/m}$, $\alpha_{\text{TD}}=68.25^\circ$; the initial states: $z_0=0.9257 \text{ m}$, $v_0=0.995 \text{ m/s}$, $\delta_0=0$; the control parameters: $k_{p1}=150$, $k_{d1}=30$, $k_{p2}=2.5$ and $k_{d2}=0.18$.

Fig. 12(a) is the vertical GRF time history of the test. If connect the wave trough point of M-type vertical GRF for every single step, we can find that this line also displays periodic fluctuations as the longitudinal force in Fig. 11(a). The periodic fluctuations reveal the

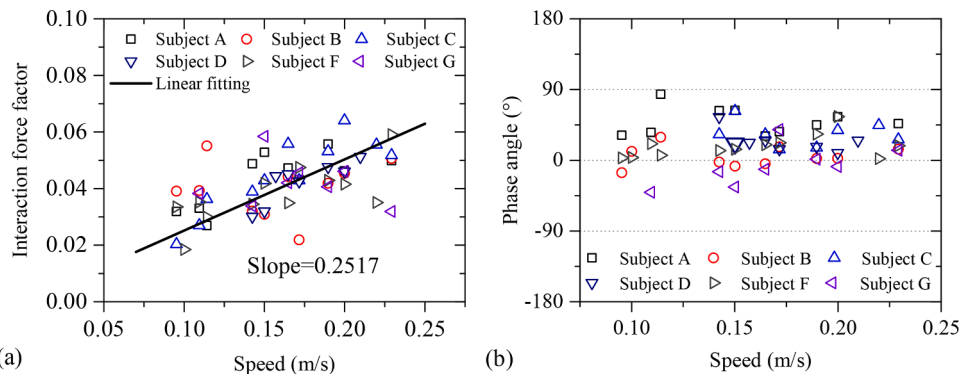


Fig. 10. Human responses during sinusoidal wave excitations; (a) interaction force amplitude and (b) phase angle.

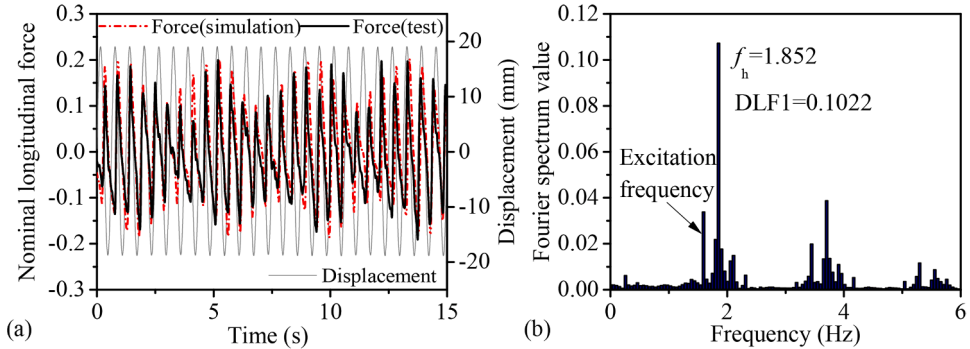


Fig. 11. Results of longitudinal force under 1.6 Hz longitudinal excitation; (a) simulation and test results and (b) Fourier spectrum of simulation.

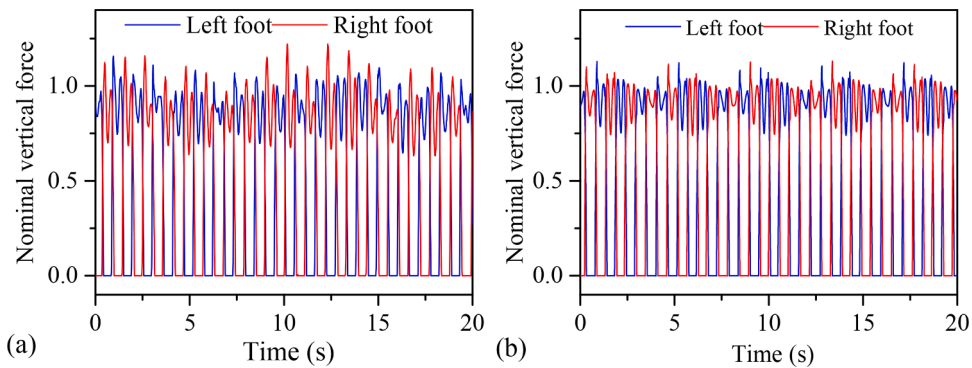


Fig. 12. Results of vertical GRF under 1.6 Hz longitudinal excitation; (a) test results and (b) simulation results.

coupling behaviors in the longitudinal and vertical directions was significant because only longitudinal excitation was applied. Meanwhile, the vertical force of the left and right feet had slight differences. The comparison of the simulation (Fig. 12(b)) and test (Fig. 12(a)) demonstrates that the change trend and the profile of the vertical force are consistent, so the model can reflect the coupling in longitudinal and vertical directions well. This suggests that the BSLIP model performs better compared to the conventional mass-

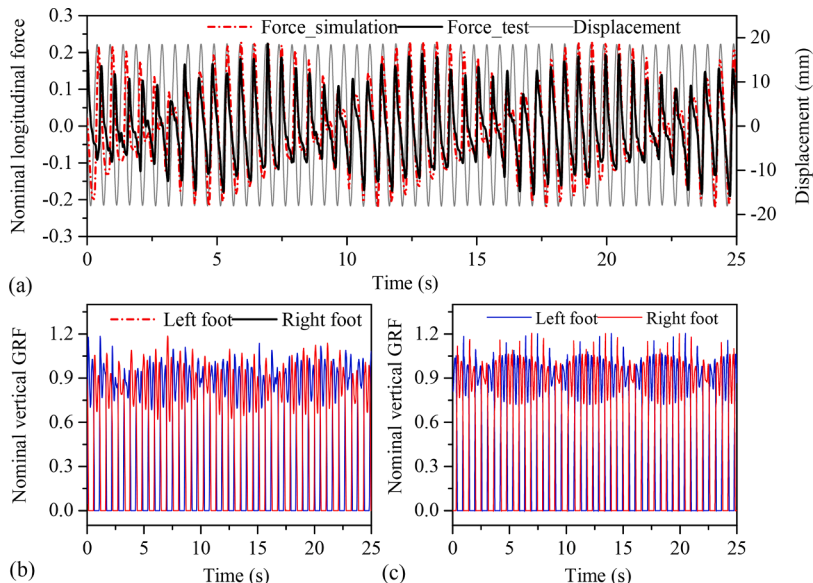


Fig. 13. Simulation and test results under 2.0 Hz longitudinal excitation; (a) simulation and test results of longitudinal force, (b) test results of vertical GRF, and (c) simulation results of vertical GRF.

spring-damping (MSD) model which models a human separately in different directions. In the test, fluctuations of the vertical force had variations in different beating periods owing to the intra-subject variability while the simulation does not present such variations.

3.3.3.2. Excitation frequency is higher than step frequency. When the excitation frequency is 2.0 Hz higher than the step frequency, the test and simulation results of the longitudinal force are shown in Fig. 13(a). In the test, the measured displacement and acceleration amplitudes were 18.4 mm and 2.9 m/s², respectively. The periodic fluctuations of vertical GRF were more obvious, and the change trend was matched with the longitudinal force, as shown in Fig. 13(b). The parameters adopted in the simulation: $k_{\text{leg}}=23 \text{ kN/m}$, $\alpha_{\text{TD}}=68.04^\circ$, the initial states: $z_0=0.9263 \text{ m}$, $v_0=0.995 \text{ m/s}$, $\delta_0=0$, and the control parameters are the same as above.

3.3.4. Synchronization

The step frequency tended to change to the same frequency as the excitation and the participant reached a state of so-called synchronization, when the initial step frequency (i.e., step frequency before excitation) was close to the excitation frequency. It can be observed that the longitudinal force lags the excitation displacement by a fixed phase angle once a participant is in synchronization. Fig. 14 shows the synchronizations for participant G under 15 mm and 20 mm excitations, and the longitudinal force in Fig. 14(b) did lag the excitation displacement by a fixed phase angle of 41.3° after 10 s (initial phase angle 162°). Since the longitudinal force is not a perfect sinusoidal wave, the phase angle difference in the positive and negative directions can be observed. It can be observed from Table 2 that the synchronization scenario in the tests occurred 10 times at 20 mm excitation while 5 times at 15 mm excitation, and the range of ratio between the initial step frequency to the step frequency at synchronization was larger at 20 mm excitation ([0.976, 1.041] for 15 mm excitation and [0.871, 1.001] for 20 mm excitation), so the probability of synchronization increased with vibration displacement amplitude. The synchronization includes two situations: one is that synchronization always keeps during test remarked as 'Persistent'; the other is that the synchronization will not be maintained after a few seconds, i.e., the synchronization is intermittent.

4. Real-time hybrid testing

4.1. Principle of RTHT

In the conventional RTHT, a part of the structure with complex mechanical behaviors is taken as the experimental substructure and the remaining part is taken as the numerical substructure. For RTHT of the HSI system, the human behaviors are much more complicated than that of the building structure. Therefore, the human is loaded on the shaking table as the experimental subsystem, while the structure is simulated in the computer as the numerical subsystem. The schematic diagram of the RTHT is shown in Fig. 15; also shown in the figure is the hardware used in the RTHT.

The equation of motion of a single-degree-of-freedom structure subjected to an earthquake and pedestrian's walking force can be expressed as

$$m_s a + c_s v + k_s u = -m_s a_g + F_h \quad (24)$$

where m_s , c_s , and k_s are the structural mass, damping coefficient, and stiffness, respectively; a , v , and u are the structural acceleration, velocity, and displacement relative to the ground, respectively; a_g denotes the ground acceleration; F_h denotes the pedestrian's longitudinal walking force exerting on the structure. Eq. (24) can be discretized by the time integration method. At an integration time step, the data acquisition computer collects human walking force in real-time, and solves absolute displacement of the structure. Then the displacement command is sent to the controller and the actuator drives the shaking table to complete loading in displacement

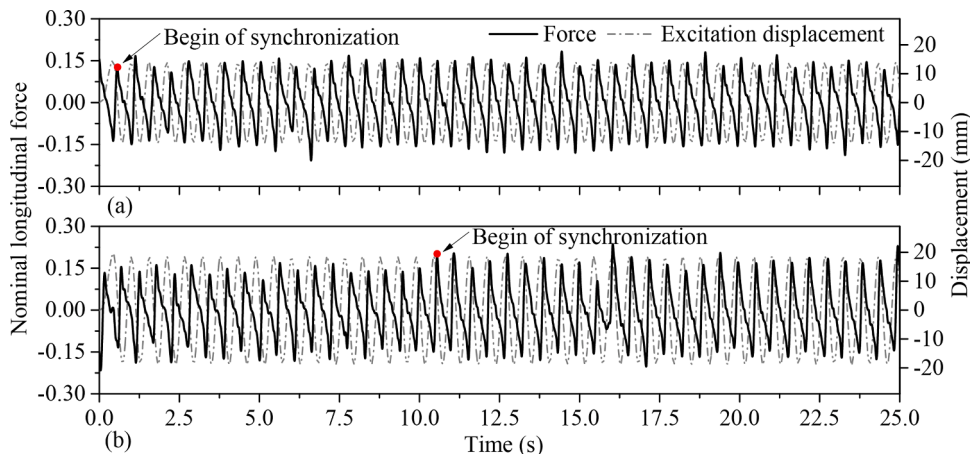
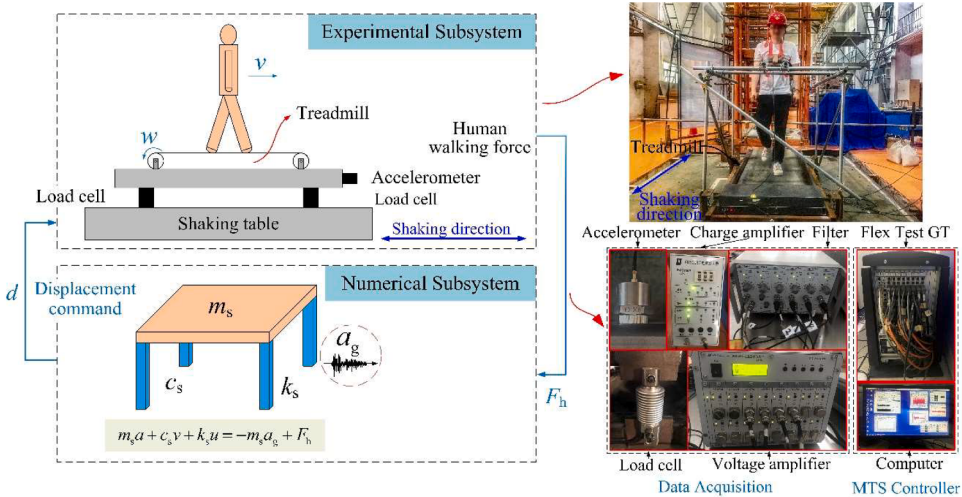


Fig. 14. Synchronization time histories of the walking force for participant G; (a) excitation with frequency of 1.8 Hz and displacement amplitude of 15 mm, (b) excitation with frequency of 1.8 Hz and displacement amplitude of 20 mm.

Table 2

Phase angle during synchronization.

Participant	Excitation amplitude (mm)	Initial step frequency (Hz)	Excitation frequency (Hz)	Positive phase (°)	Negative phase (°)	Average phase (°)	Remark
A	15	1.802	1.8	-179.6	-66.4	-123.0	Persistent
	20	1.744	1.8	-35.5	62.7	13.6	Persistent
		1.755	1.9	6.4	97.4	51.9	Intermittent
B	15	1.873	1.8	-140.9	-34.9	-87.9	Persistent
	20	1.781	1.8	-96.1	9.6	-43.3	Intermittent
		1.784	1.9	92.2	205.6	148.9	Intermittent
C	15	1.800	1.8	-130.1	-30.8	-80.4	Persistent
D	20	1.783	1.9	-30.9	68.7	18.9	Persistent
		1.741	2.0	32.0	137.8	84.9	Persistent
F	15	1.819	1.8	-124.6	-24.3	-74.5	Persistent
	20	1.801	1.8	-4.5	81	38.2	Persistent
		1.801	1.9	40.8	149.5	95.0	Persistent
G	15	1.756	1.8	93.9	192.1	143.0	Persistent
	20	1.793	1.8	41.3	147.2	94.2	Persistent
		1.803	1.9	82.5	192.6	137.6	Persistent

**Fig. 15.** The principle of shaking table hybrid test.

mode. The above process is repeated at each integration time step to fulfill the RTHT of the entire time history.

4.2. Test system

4.2.1. Hardware configuration

In the test, the shaking table was unidirectional with a maximum loading acceleration of 1.2 g, and its controller was MTS FlexTest GT with the supporting software system of MTS793. The force signals measured from the load cells and the acceleration signal were fed to the DH3840 voltage amplifier and the KD5008C charge amplifier respectively, followed by signal filtering via YE3762A and final data acquisition by MTS controller. The photographs of MTS controller and data acquisition are also shown in Fig. 15.

4.2.2. Software configuration

The synchronization of data between software and hardware is crucial for ensuring the success of the RTHT. Because the sampling frequency of the hardware for the RTHT of this study was 2048 Hz, the data sampling frequency of Calculation Editor module in MTS793 was also 2048 Hz for synchronization, which indicated that calculation for each time integration step performed by Calculation Editor must be completed within the time interval $\delta t = 1/2048$ s. The Calculation Editor may not be able to complete one calculation in δt when at a large calculation quantity. Therefore, the calculation program should be simplified as much as possible. In this study, the integration time interval was set as $\Delta t = 1/102.4$ s, which was not equal to δt . Thus, the 1-0 square wave signal was used for the time difference coordination [32], i.e., the program ran 20 times in the Calculation Editor within Δt , while the solution of the equation of motion performed only once.

4.2.3. Time integration method

Since the central difference method (CDM) [33] is an explicit integration method with good accuracy and stability, it is widely used in the RTHT and thereby was adopted for this study. The velocity and acceleration of the CDM at the n th step are

$$\begin{cases} v_n = \frac{u_{n+1} - u_{n-1}}{2\Delta t} \\ a_n = \frac{u_{n+1} - 2u_n + u_{n-1}}{\Delta t^2} \end{cases} \quad (25)$$

where subscript n denotes the integration time step. Substituting Eq. (25) into the discretized equation of motion (Eq. (24)) of the n th step, we obtain

$$u_{n+1} = \left[\frac{m_s}{\Delta t^2} + \frac{c_s}{2\Delta t} \right]^{-1} \left[\left(\frac{2m_s}{\Delta t^2} - k \right) u_n - \left(\frac{m_s}{\Delta t^2} - \frac{c_s}{2\Delta t} \right) u_{n-1} - m_s a_{g,n} + F_{h,n} \right] \quad (26)$$

The structural displacement u_{n+1} was superimposed by the ground displacement to form the absolute displacement $u_{a,n+1}$ when sent to the shaking table. The command displacement u_c was a step signal equal to u_a without time delay compensation. To obtain explicit velocity and acceleration of the $(n+1)$ th step and to drive the shaking table smoothly, the command was interpolated according to the sampling frequency. Hence a second-order polynomial interpolation based on the assumption of constant acceleration was employed. The acceleration at the n th step with an explicit expression [33] was adopted herein for the interpolation. Accordingly, the command displacement u_c of the j th substep of the $n+1$ step was

$$u_{c,n+1}^j = u_{c,n} + v_n(j\delta t) + \frac{1}{2}\tilde{a}_{n+1}(j\delta t)^2 \quad (27)$$

where \tilde{a}_{n+1} was the assumed acceleration. With

$$v_n = \frac{u_{c,n+1} - u_{c,n-1}}{2\Delta t} \quad (28)$$

when $j\delta t = \Delta t$, $u_{c,n+1}^j = u_{c,n+1}$, we had

$$\tilde{a}_{n+1} = a_n = \frac{u_{c,n+1} - 2u_{c,n} + u_{c,n-1}}{\Delta t^2} \quad (29)$$

To ensure the safety of participants and test equipment, the protective limits of 60 mm and 9 m/s² were set for command displacement and acceleration, respectively.

4.2.4. System verification

Although the ground acceleration and ground displacement files were set to be read simultaneously in the MPT module, these signals entered channels at different times with inconstant time differences in each test and introduced errors to the test. Therefore, the ground acceleration was input in MPT, while the ground displacement, instead of being input to MPT, was integrated by the acceleration in the Calculation Editor. The command displacement was an integration time interval ahead of the acceleration, which means it can exactly compose the absolute displacement in the $(n+1)$ th step when superimposed by Eq. (26).

For quantitative evaluation, a correlation coefficient and root-mean-square error (RMSE) are defined as

$$K_{xy} = \sum_{n=1}^N X_n Y_n \Bigg/ \sqrt{\sum_{n=1}^N X_n^2 \sum_{n=1}^N Y_n^2} \times 100\% \quad RMSE = \sqrt{\sum_{n=1}^N (X_n - Y_n)^2} \Bigg/ N \quad (30)$$

where X_n and Y_n are the signals to be compared and N is the number of data points.

Firstly, the RTHT was conducted on an empty structure, that is, no participant walked on the treadmill, to test the effect of factors such as system error, measurement error, and noise on the RTHT. In the RTHT, the structure had a mass, frequency, and damping ratio of 1400 kg, 1.8 Hz, and 0.05 respectively, and El Centro (EW, 1938) [34] record scaled to 300 Gal was chosen as the ground motion. The desired structural displacement relative to the ground of the RTHT was compared to the displacement of the numerical simulation (NS). It is found that the amplitude deviation $|A-A_0|/A_0$ was 1.41 %, where A and A_0 are the peak displacement of the RTHT and NS, respectively. Additionally, K_{xy} and $RMSE$ were also determined to be 0.9999 and 0.1587, respectively. These results suggest that the displacement of the RTHT agreed with that of the NS, so the effects of system error, sensor error, and noise were minimal.

Then, the RTHT that took sandbags with equal mass as the participant as the experimental subsystem was conducted to obtain the relative displacement. These quantization coefficients can also be computed as $K_{xy}=0.9898$, $RMSE=1.1423$, and amplitude deviation of 3.03 %. The difference between results of the RTHT and NS was mainly caused by the shaking table time delay. For the RTHT of inertial mass, the time delay is equivalent to the damping [35], so the displacement is smaller than the NS.

4.2.5. Time delay compensation

The shaking table was controlled by the conventional PID method, and a comparison of command and measured displacement showed a time delay of 30 ms and decay in amplitude. To consider the effect of shaking table performance, the transfer function of the shaking table was considered in the following form

$$T_A(s) = \frac{\omega_A^2}{s^2 + 2\xi_A\omega_A s + \omega_A^2} \quad (31)$$

where ξ_A and ω_A are parameters with the identified values $\xi_A=0.8628$ and $\omega_A=58.2262$. The comparison between the simulated displacement and the actual displacement of the shaking table demonstrates that the established transfer function can reflect the actual performance of the shaking table well. The inverse model compensation method was used for addressing the time delay and its performance is shown in Fig. 16. From the enlarged figure, it can be seen that the time delay between the actual and desired displacements was eliminated.

4.3. Results of RTHT for HSI system and model validation

In the RTHT of HSI system, a participant walked on the treadmill at the speed of 1.07 m/s as shown in Fig. 15. The mass and damping ratio of the structure were 1400 kg and 0.05 respectively, the mass of the participant was 71 kg, and thus the mass ratio between human to structure was 5.07 %, within a common mass ratio range for teaching buildings. Other mass ratios can also be considered by multiplying the measured longitudinal force by the corresponding scale factor. The flow of each test was as follows.

At $t=0$, the ground motion entered the channel of the MPT module and the structural response was calculated in the Calculation Editor. Meanwhile, the human longitudinal force was also collected and applied to calculate the structural response. After 30 s, the ground motion ended, but the participant continued walking and the structure vibrated under the participant's walking force until the test stopped at 60 s.

For the case with structural frequency of 1.8 Hz and the peak ground acceleration (PGA) scaled to 220 Gal, the responses of structure and participant are shown in Fig. 17, in which the structural absolute displacement of the empty structure is computed by the NS and the displacement that participant walking on the structure was obtained by the RTHT (indicated by 'Occupied structure'). The results show that human walking had obvious influences on the structural response, and the peak displacement was 11.3 % less than that of the empty structure. Fig. 17(b) is step frequency in which the average step frequency of the left and right feet is taken. It can be seen the step frequency represented an increase when the participant subjected to the shaking table excitation. From wavelet analysis of the structural displacement (Fig. 17(c)), although the initial step frequency was similar to the structural fundamental frequency, the structure vibration frequency was dispersed around 1.8 Hz, making the participant difficultly adjust the step frequency to be consistent with the structural vibration frequency.

For the case with structural frequency of 2.0 Hz and PGA of 220 Gal, the maximum structural absolute displacement was 0.12 % smaller than that of the empty structure, but structural response for the latter was significantly larger, as shown in Fig. 18(a). The Fourier transforms of the structural displacement for the empty structure and occupied structure are shown in Fig. 18(d). It can be computed that the component at 2 Hz increases by 48.3 % compared with the empty structure case, which showed that the response at the fundamental frequency increased significantly. From Fig. 18(b), the step frequency still increased after the seismic wave entered and continuously adjusted, and finally maintained near 2 Hz corresponding to the structural vibration frequency. This is also demonstrated by Fig. 18(c), which shows the longitudinal force and the structural displacement during the earthquake, and the human motion was synchronized with the structural motion. The time-frequency diagram of wavelet analysis on the structural displacement (in Fig. 18(e)) reveals that the structural vibration frequency was always distributed around 2 Hz, which was the same as the step frequency.

By combining Eqs. (11), (16), and (24), we can obtain equations of human-structure interaction system. Then we can perform the simulation of the HSI system to obtain the seismic response as shown in Fig. 19. Although BSLIP has some drawbacks, such as the variation of step frequency in the simulation is not significant as in the test, the model performs well, which proves that it can simulate the seismic response of HSI system. The parameters adopted in the simulation: $k_{leg}=23$ kN/m, $\alpha_{TD}=69.81^\circ$, the initial states: $z_0=0.9229$ m, $v_0=0.995$ m/s, $\delta_0=0$, and the control parameters are the same as above.

The results of RTHT under different test conditions, tabulated in Table 3, show that the maximum structural seismic displacements

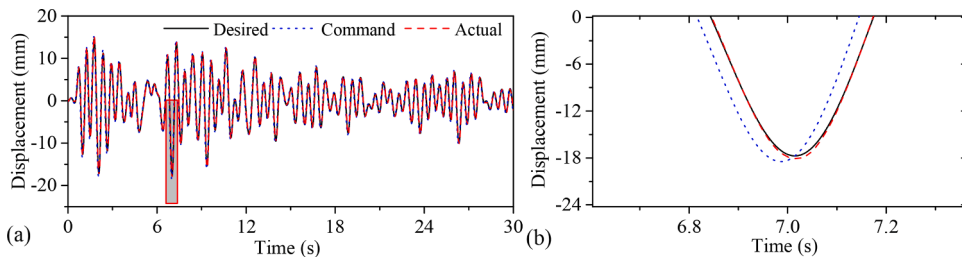


Fig. 16. Delay compensation results; (a) comparison of displacement response and (b) partially enlarged view.

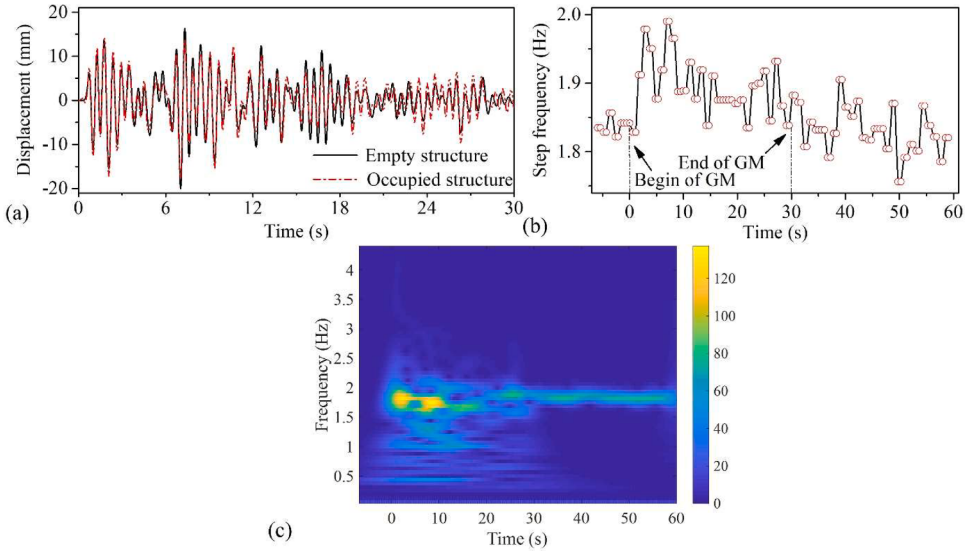


Fig. 17. Results of RTHT with structural frequency of 1.8 Hz and PGA of 220 Gal; (a) structural displacement response, (b) step frequency, and (c) results of wavelet analysis. (Note: GM denotes ground motion).

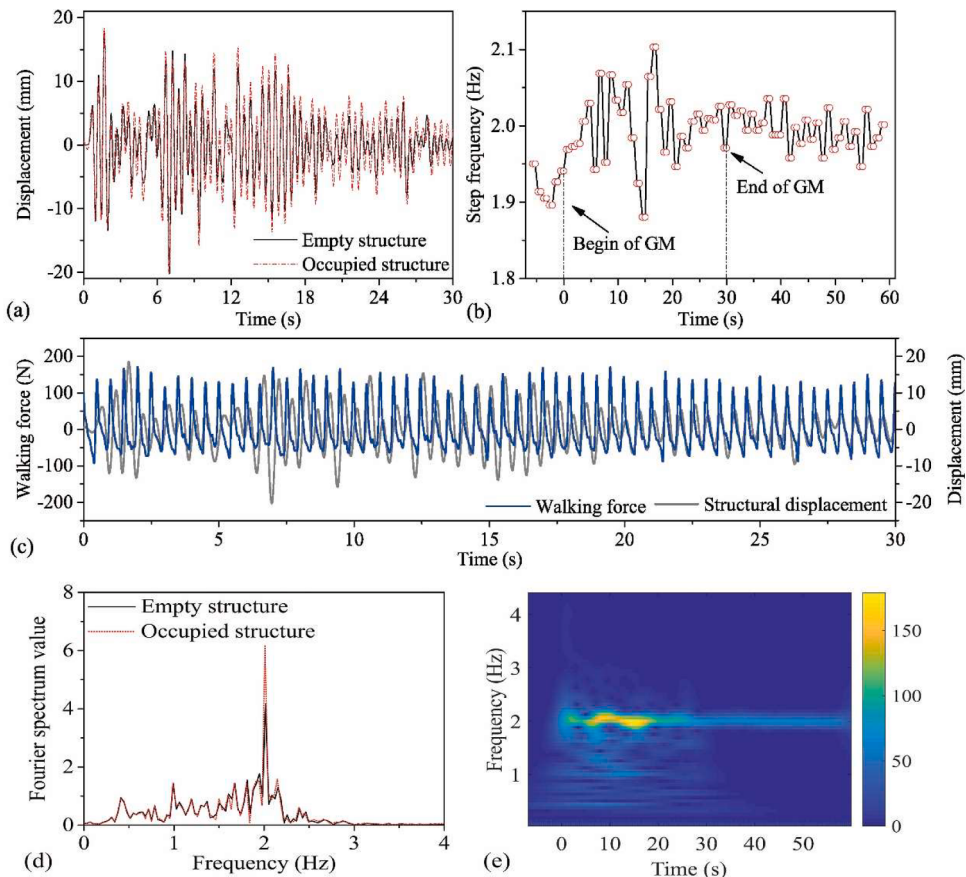


Fig. 18. Results of hybrid test with structural frequency of 2.0 Hz and PGA of 220 Gal; (a) structural displacement response, (b) step frequency, (c) walking force and structural vibration displacement, (d) comparison of Fourier spectrum, and (e) results of wavelet analysis.

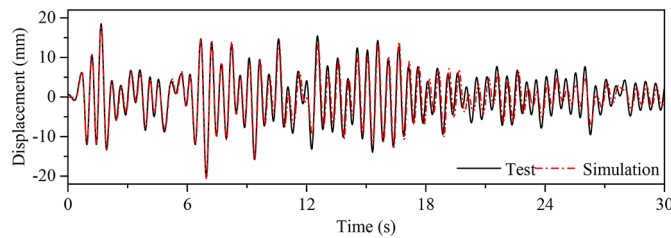


Fig. 19. Response comparison between test and simulation with structural frequency of 2.0 Hz and PGA of 220 Gal.

Table 3

RTHT results of human-structure interaction system with mass ratio 5.07 % and damping ratio 5 %.

Structural frequency (Hz)	1.8				1.6	2.0	
Peak ground acceleration (Gal)	220	300	300	300	300	220	300
$ A - A_0 /A_0$ (%)	-11.3 (1.84)	-3.27 (1.89)	-3.38 (1.93)	-14.7 (1.80)	0.8 (1.89)	-0.12 (1.92)	-5.57 (1.92)
Average step frequency (Hz)	1.89 (1.83)	1.92 (1.85)	1.96 (1.96)	1.81 (1.82)	1.93 (1.86)	2.00 (2.00)	2.02 (1.93)

Note that A and A_0 represent the peak displacement of the occupied structure and its corresponding empty structure.

in the presence of human were mostly reduced compared to the displacement of empty structure. The adverse effects of human walking on the structural peak displacement were insignificant due to the small mass ratio between human and structure. However, the risk of displacement amplification improved with the increase of mass ratio, and this was demonstrated by the case at mass ratio of 10.14 % in which the displacement of occupied structure was greater than that of the empty structure by 8.62 % with the structure frequency of 1.8 Hz and the ground motion scaled to 300 Gal. In the average step frequency row, step frequencies before and after the entry of the ground motion are shown in parentheses. The step frequency tended to increase when subjected to the ground excitation and generally returned to its previous level after the record ended. It can also be found that the step frequencies were adjusted to around 2 Hz during the earthquake when the structural frequency is 2.0 Hz near the main frequency of the ground motion.

As a result, the motion of human body may either enhance or weaken the structural response. Specifically, the structural vibration concentrates on the excitation frequency when the structural frequency is equal to the main frequency of the ground record. Meanwhile, if the step frequency is close to the vibration frequency, the participants tend to adjust their step frequency to synchronize with the structural vibration and it might cause a remarkable increase in the structural response. In comparison, the influence of human is small when the structure frequency is far from the step frequency. Note that although only a single participant walked on the treadmill during the test, the RTHT can also be applied to the research of multi-participant-structure interaction by increasing the number of participants on the shaking table in the future. Meanwhile, the proposed BSLIP model can also be further adopted for the investigation of crowd-structure interaction issues by introducing the social force model [17].

5. Conclusions

This study mainly focuses on the modeling and response investigation of the HSI system, and the main conclusions are written as follows.

- (1) The HSI in the longitudinal direction can be interpreted as additional positive mass and positive damping contribution to the occupied structure. The human may adjust the step frequency to be synchronized with structural vibration when the step frequency is close to the excitation frequency.
- (2) The BSLIP model can represent the non-synchronization and synchronization responses of the human body on the longitudinally vibrating surfaces, and simulation results are consistent with the tests in terms of the walking force amplitudes and phase lags. Meanwhile, the model can also reflect the coupling behavior in the longitudinal and vertical directions. The comparison with RTHT results demonstrates the established model can be applied to evaluate the seismic response of the HSI system.
- (3) The RTHT results showed the step frequencies changed significantly when subjected to ground vibration and human movement may enhance or weaken the structural response. Synchronization might occur when the step frequency is close to the structural vibration frequency, causing a significant effect on the structural seismic response.

CRediT authorship contribution statement

Haowen Yang: Conceptualization, Data curation, Formal analysis, Investigation, Methodology, Software, Writing – original draft, Writing – review & editing. **Bin Wu:** Conceptualization, Funding acquisition, Project administration, Supervision, Writing – original draft, Writing – review & editing. **Guoshan Xu:** Funding acquisition, Project administration, Resources.

Declaration of competing interest

The authors declare that they have no known competing financial interests or personal relationships that could have appeared to influence the work reported in this paper.

Data availability

Data will be made available on request.

Acknowledgements

This research is funded by the National Natural Science Foundation of China (Grant Nos. 51878525, 52278211, 52308194 and 51978213), the Major Science and Technology Project of Hainan Province (Grant No. ZDKJ2021024) and the Sanya Science and Education Innovation Park of Wuhan University of Technology (Grant No. 2021KF0006). The support is greatly acknowledged.

References

- [1] V. Racic, A. Pavic, J.M.W. Brownjohn, Experimental identification and analytical modelling of human walking forces: literature review, *J. Sound Vib.* 326 (2009) 1–49, <https://doi.org/10.1016/j.jsv.2009.04.020>.
- [2] P. Dallard, A.J. Fitzpatrick, A. Flint, S. Le Bourva, A. Low, R.M. Ridsill Smith, M. Willford, The London millennium footbridge, *Struct. Eng.* 79 (2001) 17–33.
- [3] I. Belykh, M. Bocian, A.R. Champneys, K. Daley, R. Jeter, J.H.G. Macdonald, A. McRobie, Emergence of the London Millennium Bridge instability without synchronization, *Nat. Commun.* 12 (2021) 1–14, <https://doi.org/10.1038/s41467-021-27568-y>.
- [4] Z.L. Liu, M.F. Wang, F. Liao, Research on dynamic performance of reinforced concrete frame teaching building considering the influences of pedestrian incentive load, *J. Hunan. Univ. (Nat. Sci.)* 44 (2017) 86–96 (In Chinese).
- [5] B.R. Ellis, T. Ji, Human-structure interaction in vertical vibrations, *Proc. Inst. Civil. Eng.-Struct. Build.* 122 (1997) 1–9, <https://doi.org/10.1680/istbu.1997.29162>.
- [6] Y. Matsumoto, M.J. Griffin, The horizontal apparent mass of the standing human body, *J. Sound Vib.* 330 (2011) 3284–3297, <https://doi.org/10.1016/j.jsv.2011.01.030>.
- [7] S. Živanović, I.M. Diaz, A. Pavic, Influence of walking and standing crowds on structural dynamic properties, in: Proceeding of conference & exposition on structural dynamics (IMAC XXVII), Orlando, USA, 2009.
- [8] H.V. Dang, S. Živanović, Influence of low-frequency vertical vibration on walking locomotion, *J. Struct. Eng.* 142 (2016) 4016120, [https://doi.org/10.1061/\(ASCE\)ST.1943-541X.0001599](https://doi.org/10.1061/(ASCE)ST.1943-541X.0001599).
- [9] H. Geyer, A. Seyfarth, R. Blickhan, Compliant leg behaviour explains basic dynamics of walking and running, *Proc. R. Soc. B* 273 (2006) 2861–2867, <https://doi.org/10.1098/rspb.2006.3637>.
- [10] B.R. Whittington, D.G. Thelen, A simple mass-spring model with roller feet can induce the ground reactions observed in human walking, *J. Biomech. Eng.* 131 (2009) 011013, <https://doi.org/10.1115/1.3005147>.
- [11] J.W. Qin, S.S. Law, Q.S.N. Yang, Pedestrian–bridge dynamic interaction, including human participation, *J. Sound Vib.* 332 (2013) 1107–1124, <https://doi.org/10.1016/j.jsv.2012.09.021>.
- [12] B.T. Lin, Q.W. Zhang, F. Fan, S.Z. Shen, A damped bipedal inverted pendulum for human-structure interaction analysis, *Appl. Math. Model.* 87 (2020) 606–624, <https://doi.org/10.1016/j.apm.2020.06.027>.
- [13] J.H.G. Macdonald, Lateral excitation of bridges by balancing pedestrians, *Proc. R. Soc. A* 465 (2009) 1055–1073, <https://doi.org/10.1098/rspa.2008.0367>.
- [14] S.P. Carroll, J.S. Owen, M.F.M. Hussein, Experimental identification of the lateral human–structure interaction mechanism and assessment of the inverted-pendulum biomechanical model, *J. Sound Vib.* 333 (2014) 5865–5884, <https://doi.org/10.1016/j.jsv.2014.06.022>.
- [15] V. Joshi, M. Srinivasan, Walking crowds on a shaky surface: stable walkers discover Millennium Bridge oscillations with and without pedestrian synchrony, *Biol. Lett.* 14 (2018) 20180564, <https://doi.org/10.1098/rsbl.2018.0564>.
- [16] P.F. Tang, M.H. Woollacott, R. Chong, Control of reactive balance adjustments in perturbed human walking: roles of proximal and distal postural muscle activity, *Exp. Brain Res.* 119 (1998) 141–152, <https://doi.org/10.1007/s002210050327>.
- [17] D. Helbing, P. Molnar, Social force model for pedestrian dynamics, *Phys. Rev. E* 51 (1995) 4282, <https://doi.org/10.1103/PhysRevE.51.4282>.
- [18] S.P. Carroll, J.S. Owen, M.F.M. Hussein, A coupled biomechanical/discrete element crowd model of crowd–bridge dynamic interaction and application to the Clifton Suspension Bridge, *Eng. Struct.* 49 (2013) 58–75, <https://doi.org/10.1016/j.engstruct.2012.10.020>.
- [19] M. Nakashima, H. Kato, E. Takaoka, Development of real-time pseudo dynamic testing, *Earthq. Eng. Struct. Dyn.* 21 (1992) 79–92, <https://doi.org/10.1002/eqe.4290210106>.
- [20] T. Horiuchi, M. Inoue, T. Konno, W. Yamagishi, Development of a real-time hybrid experimental system using a shaking table:(proposal of experiment concept and feasibility study with rigid secondary system), *JSME Int. J. Ser. C* 42 (1999) 255–264, <https://doi.org/10.1299/jsmec.42.255>.
- [21] J.T. Wang, Y. Gui, F. Zhu, F. Jin, M.X. Zhou, Real-time hybrid simulation of multi-story structures installed with tuned liquid damper, *Struct. Control Health Monit.* 23 (2016) 1015–1031, <https://doi.org/10.1002/stc.1822>.
- [22] G.S. Xu, Y. Ding, J.F. Xu, Y.S. Chen, B. Wu, A shaking table substructure testing method for the structural seismic evaluation considering soil-structure interactions, *Adv. Struct. Eng.* 23 (2020) 3024–3036, <https://doi.org/10.1177/1369433220927267>.
- [23] Z.Y. Tang, H. Liu, M. Dietz, C.T. Chatzigogos, X.L. Du, Nonlinear behavior simulation of soil-structure interaction system via real-time hybrid testing, *Bull. Earthq. Eng.* 20 (2022) 6109–6128, <https://doi.org/10.1007/s10518-022-01429-5>.
- [24] W. Guo, Y. Wang, C. Zeng, T. Wang, Q. Gu, H.M. Zhou, L.Y. Zhou, W.Q. Hou, Moving safety evaluation of high-speed train on post-earthquake bridge utilizing real-time hybrid simulation, *J. Earthq. Eng.* 27 (2023) 284–313, <https://doi.org/10.1080/13632469.2021.1999869>.
- [25] H.W. Yang, B. Wu, J.P. Li, Y. Bao, G.S. Xu, A spring-loaded inverted pendulum model for analysis of human-structure interaction on vibrating surfaces, *J. Sound Vib.* 522 (2022) 116727, <https://doi.org/10.1016/j.jsv.2021.116727>.
- [26] L.C. Visser, S. Stramigioli, R. Carloni, Robust bipedal walking with variable leg stiffness, in: Proceedings of the IEEE RAS/EMBS International Conference on Biomedical Robotics and Biomechatronics, Roma, Italy, 2012, pp. 1626–1631.
- [27] F. Ricciardelli, A.D. Pizzimenti, Lateral walking-induced forces on footbridges, *J. Bridg. Eng.* 12 (2007) 677–688, [https://doi.org/10.1061/\(ASCE\)1084-0702\(2007\)12:6\(677\)](https://doi.org/10.1061/(ASCE)1084-0702(2007)12:6(677)).
- [28] E.T. Ingólfsson, C.T. Georgakis, F. Ricciardelli, J. Jonsson, Experimental identification of pedestrian-induced lateral forces on footbridges, *J. Sound Vib.* 330 (2011) 1265–1284, <https://doi.org/10.1016/j.jsv.2010.09.034>.
- [29] P. Kumar, A. Kumar, V. Racic, Modeling of longitudinal human walking force using self-sustained oscillator, *Int. J. Struct. Stab. Dyn.* 18 (2018) 1850080, <https://doi.org/10.1142/S0219455418500803>.
- [30] H. Geyer, Simple Models of Legged Locomotion Based on Compliant Limb Behavior, PhD thesis, University of Jena, 2005.

- [31] M. Bocian, J.H.G. Macdonald, J.F. Burn, D. Redmill, Experimental identification of the behaviour of and lateral forces from freely-walking pedestrians on laterally oscillating structures in a virtual reality environment, Eng. Struct. 105 (2015) 62–76, <https://doi.org/10.1016/j.engstruct.2015.09.043>.
- [32] Q.Y. Wang, Real-Time Substructure Testing Method and Its Application, PhD thesis, Harbin Institute of Technology, 2007.
- [33] B. Wu, L.X. Deng, X.D. Yang, Stability of central difference method for dynamic real-time substructure testing, Earthq. Eng. Struct. Dyn. 38 (2009) 1649–1663, <https://doi.org/10.1002/eqe.927>.
- [34] PEER (Pacific Earthquake Engineering Research Center), Pacific earthquake engineering research center strong motion database, 2016. <https://ngawest2.berkeley.edu/> (accessed 31 July 2023).
- [35] F. Chi, J. Wang, F. Jin, Delay-dependent stability and added damping of SDOF real-time dynamic hybrid testing, Earthq. Eng. Eng. Vib. 9 (2010) 425–438, <https://doi.org/10.1007/s11803-010-0026-0>.